Results in Physics 18 (2020) 103222

Contents lists available at ScienceDirect

Results in Physics

journal homepage: www.elsevier.com/locate/rinp

Interface electronic structure between aluminum and black phosphorus

Baoxing Liu[a,b], Haipeng Xie[a,*], Dongmei Niu[a], Shitan Wang[a], Yuan Zhao[a], Yuquan Liu[a], Yongli Gao[c,a]

[a] Hunan Key Laboratory for Super-microstructure and Ultrafast Process, School of Physics and Electronics, Central South University, Changsha, Hunan 410012, PR China
[b] College of Physics and Optoelectronic Engineering, Shenzhen University, Shenzhen 518060, PR China
[c] Department of Physics and Astronomy, University of Rochester, Rochester 14627, USA

ARTICLE INFO

Keywords:
Black phosphorus
Aluminum
Photoemission spectroscopy
Electronic structure

ABSTRACT

The electronic properties of the interface between Al and black phosphorus were studied by photoemission spectroscopy (PES). We observed that the growth pattern of Al deposited onto the BP film is Stranski-Krastanov mode. There is a reaction between Al atoms and P atoms at the interface and forming Al-P compounds, which changes the interface barriers and impedes carrier transfer. It is suggested that an inert buffer layer is necessary to protect BP and lower the carrier barriers to develop Al/BP-based device with high performance.

Introduction

2D materials are extensively studied because of their special geometric structures and physicochemical properties. Graphene is the forefather of 2D materials, which has high carrier mobility and outstanding physical properties [1–6]. However, its potential functionalities and applications are limited due to the zero-band gap characteristics of graphene [7]. As a fast emerging 2D material, black phosphorus (BP) has become a research hotspot due to its remarkable photoelectric properties [8–14]. Like graphite, BP has a layered structure and stack by weak van der Waals interactions. The most significant difference between BP and graphene is that BP has a band gap and its value can be adjusted with the thickness [15–17]. BP has good electrical properties at room temperature, the application potential of BP has been greatly developed [18]. BP as a 2D monoelemental materials, doping a certain VA group element in it, tuning the monoelemental crystals into bielemental, can preserve the advantages of BP's unique structures, modulate its properties, and further expand its multifunctional applications [19]. Optoelectronic devices fabricated from 2D semiconductors such as BP exhibit many-body complexes which determine the materials optical and electrical properties. Characterization and manipulation of these complexes have become a reality, further improving the performance of BP-based optoelectronic devices [20]. A variety of equipment based on BP such as the field-effect transistor, solar cells, photodetector, pulsed lasers, have proven to be viable [21–28].

One significant challenge facing BP applications is its environmental stability. The peeled BP films will degrade in the atmosphere, lead to the carrier mobility and on/off current ratio of BP decrease significantly [22,29]. Thus, in order to maintain the inherent structure and property of BP, an efficient and reliable isolation/passivation layer is needed. AlO_x overlayer protection is an effective method to passivate BP flakes from atmospheric degradation, Wood et al. reported that the BP FETs encapsulated by deposition of Al can maintain high mobilities for more than two weeks in the atmosphere [29]. Furthermore, Al_2O_3 can be used as barrier layers. Liu et al. fabricated an ambipolar BP transistor using an Al_2O_3 capping layer and the ambipolarity is obtained by reduced the Schottky barrier heights [30]. Generally, the protective and barrier layers are prepared by depositing Al on BP films and then performing thermal oxidation. Perello et al. reported a high-performance n-type BP transistor with Al contacts, the electron mobilities ranging from 10^2 to 10^3 cm^2 V^{-1} s^{-1} and $I_{on}/I_{off} > 10^5$ at room temperature. Due to the existence of a Schottky barrier at the Al-BP contact, a flake thickness dependence of dominant carrier type was also observed [31]. Liu et al. showed theoretically and experimentally the effectiveness of Al atoms as electron donors to transform the undoped p-type BP into n-type conductance [32]. Despite the fascinating device characteristics, the interface electronic structure between Al and BP is still not very clear, to better understand the behavior of the device, it is necessary to further study it.

Here, the electronic structure of the Al/BP interface was studied by PES. In our study we found that the growth pattern of Al deposited onto the BP film was in the Stranski-Krastanov mode. The Al-P compound formed at the initial deposition of Al and its amount increased gradually with increasing the Al thickness from 0 to 8 Å. Angle-resolved X-ray photoemission spectroscopy (AR-XPS) data shows that the Al-P compounds only exist at the interface and change the interface barriers,

* Corresponding author.
E-mail address: xiehaipeng@csu.edu.cn (H. Xie).

https://doi.org/10.1016/j.rinp.2020.103222
Received 24 April 2020; Received in revised form 27 June 2020; Accepted 30 June 2020
Available online 05 July 2020
2211-3797/ © 2020 The Author(s). Published by Elsevier B.V. This is an open access article under the CC BY-NC-ND license (http://creativecommons.org/licenses/by-nc-nd/4.0/).

which is harmful to carriers transport. Our study is helpful to understand the behavior of the Al/BP interface.

Materials and methods

In situ photoemission experiments were carried out in an ultrahigh vacuum system. Before the experiment, the evaporation source was degassed at appropriate temperatures. The manufacturer of BP single crystal is HQ Graphene, and it is mechanically peeled with scotch tape in the preparation room. Then, the obtained freshly cleaved bulk BP crystal was immediately transferred to the analysis chamber and the surface composition and crystal structure have been verified. Al films were grown layer by layer in MBE chamber whose pressure is about 2×10^{-10} mbar and its thickness was monitored by a quartz crystal microbalance. X-ray photoemission spectroscopy (XPS) measurement was operated with 100 meV scanning step [33]. In order to measure the secondary electrons cutoff, a − 5 V bias was applied to the sample during ultraviolet photoemission spectroscopy (UPS) measurement [34,35].

Results and discussion

Fig. 1(a) is the crystal structure of BP, Fig. 1(b) is the growth schematic representation of metals films and Fig. 1(c) is the XPS full spectra. As shown in Fig. 1(c), the peak of P 2p is located at ca. 130.24 eV, and no other peak has been detected at high binding energy, indicating that the BP has not been oxidized during mechanical exfoliation in high vacuum [36]. A clear low energy electron diffraction (LEED) pattern has been presented as shown in the inset of Fig. 1(c). Combining with the XPS and LEED data, it is found that the BP surface was successfully prepared by mechanically peeled off in the preparation chamber.

As shown in Fig. 2(a) and (b), UPS spectra of the cut-off region and the VB edge region evolve with the thickness of Al deposited on BP. For clarity of vision, all the spectra have been normalized. For the intrinsic BP, its Work Function (WF) is 4.24 eV which is consistent basically with the previous report [35]. The WF is 4.14 eV when the thickness of Al is 1 Å and decreases with the subsequent deposition, approach to the minimum 3.81 eV after the deposition of 8 Å Al. Then WF increases slowly with further increase the Al thickness and it is 4.03 eV at 60 Å. As shown in Fig. 2(b), the valence band maximum (VBM) of intrinsic BP is about 0.1 eV. When the thickness of Al reaches 30 Å, the metallic Fermi level cutoff begins to appear. Fig. 2(c) display the evolution of WF with the Al film thickness, a gradual shift was observed with the subsequent Al deposition, indicating that the interface barriers have been changed. According to the band gap (E_{gap}) of bulk BP is 0.3 eV, the conduction band minimum (CBM) of intrinsic BP calculated by formula $E_{CBM} = E_{gap} - E_{VBM}$ is 0.2 eV [8].

XPS was used to study the chemical properties of samples and investigate the reasons for the change of WF with increasing Al thickness. Shown in Fig. 3(a), (b) are P 2p and Al 2p spectra at Al film thickness from 0 to 60 Å and all the spectra have been normalized. The core level of P 2p is a doublet consisting of P $2p_{3/2}$ and P $2p_{1/2}$, and in this paper, only the P $2p_{3/2}$ peak is analyzed in detail for simplicity [36]. The translucent blue peak corresponds to the P $2p_{3/2}$ peak of intrinsic BP, the position is at 130.24 eV. With the increase of Al thickness, it remains basically unchanged. At the initial deposition of Al, a translucent red peak appeared, corresponding to Al atoms at the interface reaction with P atoms and forming Al-P compounds, the position is at 129.24 eV. Similar results were obtained by several controlled experiments. In the first controlled experiment, the surface of the bulk BP has a small amount of absorbed oxygen and the Al films were thermally evaporated in the molecular beam epitaxy chamber whose pressure is better than 1.5×10^{-10} mbar. Due to the oxygen molecules are adsorbed on the BP surface, Al ions are more easily oxidized, so the AlO_x content is greater at the initial deposition of Al, as shown in supporting information Fig. S1. It is found that the Al-P compounds content obviously increased at 4 Å and decreased at 15 Å. It indicated that the Al preferentially react with the absorbed oxygen and the formation of Al-P compounds also exist at interface region. To eliminate the interference of the equipment, we repeated the experiment using a new Al evaporation source in another evaporation chamber whose pressure is superior to 5×10^{-8} mbar, and also found the formation of Al-P compounds, as shown in Fig. S2. Results from experiments under different conditions indicate that the Al-P compounds appear at the Al/BP interface when Al is deposited on BP.

Al 2p is more complex to analyze. In Fig. 3(b), at the initial Al deposition, the Al 2p-related peaks are located at 74.24 eV and 75.72 eV, respectively. The 74.24 eV one is Al-P compounds and it gradually attenuated as the Al overlayer thickness increases. The 75.72 eV peak is from AlO_x, [37] as it has the proper separation from the metallic Al peak. With the subsequent deposition, a new peak located at 73.24 eV

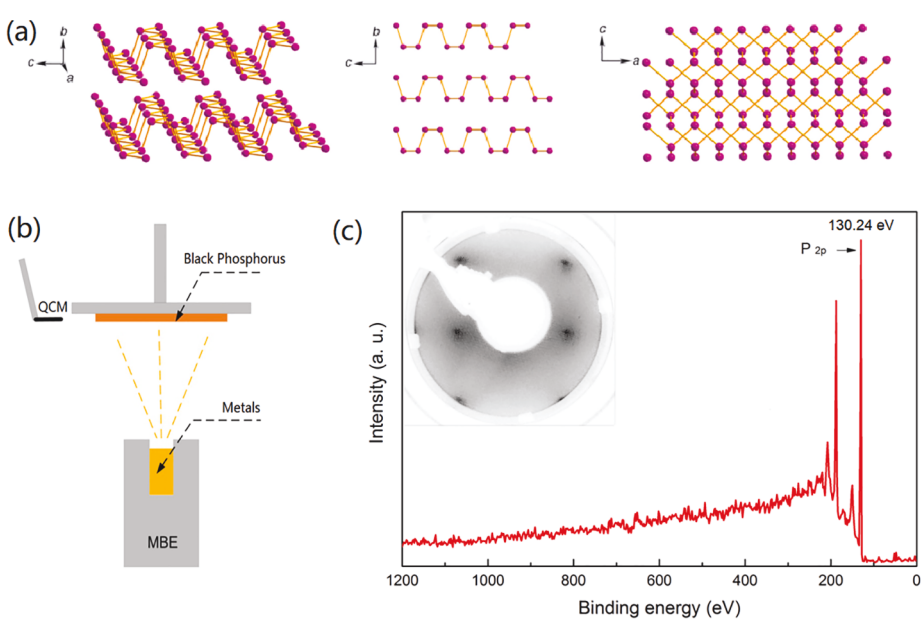

Fig. 1. (a) Crystal structure of BP. (b) Metal growth schematics. (c) XPS measurement of BP. Inset: LEED image of BP at 37 eV electron energy.

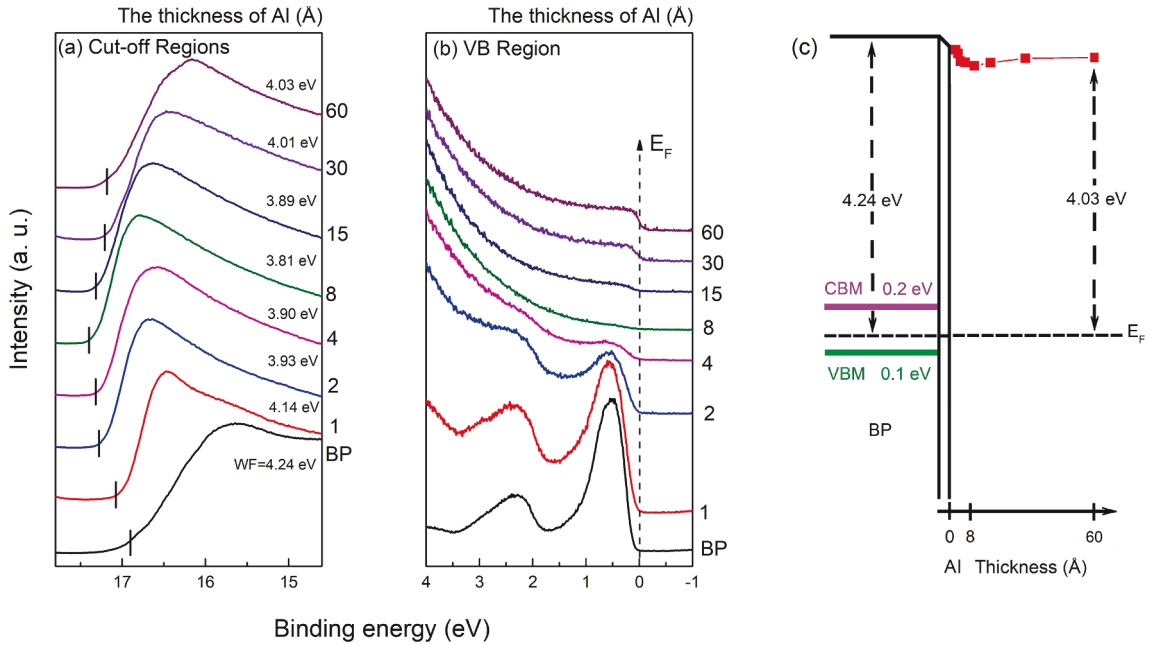

Fig. 2. UPS spectra of (a) the cut-off region, (b) the VB edge region at Al film thickness from 0 to 60 Å. (c) The evolution of work function with the Al film thickness.

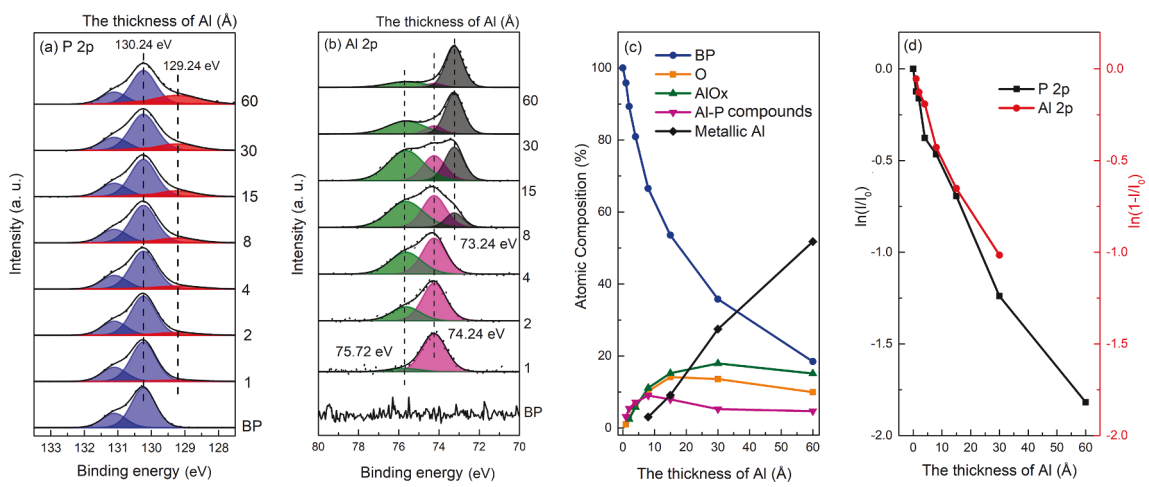

Fig. 3. (a) P 2p, (b) Al 2p spectra at Al film thickness from 0 to 60 Å. (c) Atomic concentration and (d) photoelectron intensity at Al film thickness from 0 to 60 Å.

appears at 8 Å, which can be attributed to metallic aluminum. The coverage agrees with the emergence of the Al Fermi edge in the UPS spectrum. Based on the UPS data, the most logical assumption is that the formation of aluminum oxides and Al reacts with BP at the interface which causes changes in VL. Fig. 3(c) shows the atomic concentration of all components as a function of Al thickness. To distinguish different components, the Al 2p-related peaks located at ca. 73.24 eV, 74.24 eV, and 75.72 eV is assigned to metallic Al, Al-BP compounds, and AlO_x respectively. The amount of BP decreases monotonically as the Al thickness increases. The AlO_x and O behave differently from BP, their intensities increase first and then decrease gradually with the Al thickness increase. The amount of metallic Al gradual increases as the Al thickness increases. Al-BP compounds intensities decrease obviously after 8 Å, indicating that the reaction only occurs at 0–8 Å. The Al-P compounds exists at the Al/BP interface, in which should change the optical properties at the interface region. However, it should be noted that this region is limited to a few nanometers in thickness, as the unreacted BP is still dominant. Combine with the UPS spectra (Fig. 2c), we find that the interface barrier has been changed by the reaction, which is not conducive to carrier transport. To eliminate the reaction and suppress the interface barrier, the buffer layer is needed between Al and BP.

To further study the growth process of Al on BP film, we analyzed the attenuation of XPS intensity by Al overlayer (I_{Al}) [38].

$$I_{Al} = I_{60} \times [1 - exp(-d/\lambda_{Al})] \quad (1)$$

or BP substrate (I_{BP})

$$I_{BP} = I_0 \times exp(-d/\lambda_{BP}) \quad (2)$$

I_0 is the photoelectron intensities from intrinsic BP, I_{60} is from 60 Å Al overlayer. d is the thickness of the Al film deposition, λ_{Al} (λ_{BP}) is the mean free path (MFP) of photoexcited electrons in Al (P) [35]. The growth pattern of Al deposited on the BP substrate can be obtained by the attenuation of the XPS peaks, which calculated by the Eqs. (1) and (2) [39]. As shown in Fig. 3 (d), between 1 and 8 Å, the curve of P 2p peak attenuation is linear, 8–60 Å, linear has slightly different slopes. This date derives an electron escape depth of ~20 Å, which is in good agreement with the expected value [40]. It is suggesting that as Al is deposited onto the BP film, the growth pattern is Stranski-Krastanov mode.

To analyze the distribution of all components, AR-XPS is used for

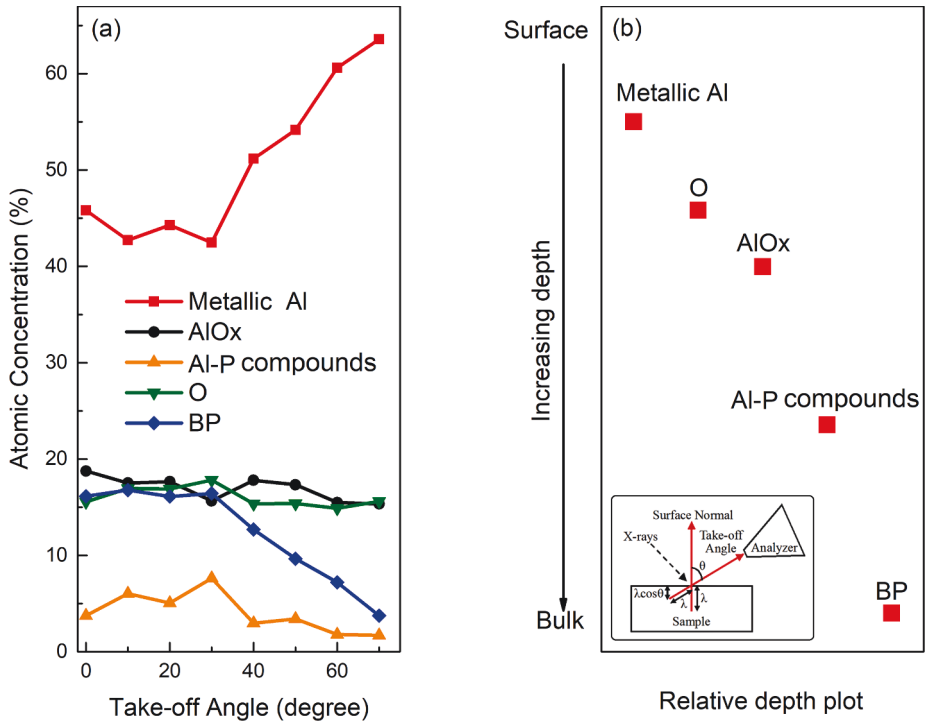

Fig. 4. In the Al/BP film, (a) atomic concentration at different takeoff angle, (b) relative depth plot of chemical components.

the 60 Å Al deposition on the BP substrate. In Fig. 4(a), the atomic concentration of all components is plotted at different takeoff angle. The inset of Fig. 4(b) illustrates the AR-XPS measurement geometry [41]. As shown in Fig. 4(a), with the takeoff angle, increased from 0 to 70°, metallic Al increased, indicates that more metallic Al is distributed at the surface than in the bulk, while BP shows an inverse distribution, agree well with the XPS results as mentioned above. O shows a homogeneous distribution in the sample. Fig. 4(b) uses the relative sensitivity of each chemical component relative to the takeoff angle to obtain an ordering of the components by depth [42]. It is observed that the BP and Al-P compounds have a greater relative depth, the O and AlO_x have moderate relative depths, and the metallic Al have the smaller relative depth for the Al/BP film. These depth observations support our assertion that Al-P compounds only exists at the interface region, which suggests that the Al react with the top layers of BP. Thus, we speculate that a monolayer BP may show a similar behavior as the bulk BP and be damaged by the reaction although it may deserve further investigations.

Conclusions

We investigated the electronic properties of the Al/BP interface and found that there is a reaction between Al and BP. Al-P compounds were formed at the initial Al deposition and it only exists at the interface region. The interface interaction would change the interface barrier and against the carriers transport. It is suggested that a buffer layer inset into the Al/BP interface is necessary. The process of the growth of Al on the BP substrate is Stranski-Krastanov mode. These observations are helpful for the performance improvement of Al/BP-based devices.

CRediT authorship contribution statement

Baoxing Liu: Investigation, Formal analysis, Visualization, Writing - original draft. **Haipeng Xie:** Conceptualization, Methodology, Writing - review & editing. **Dongmei Niu:** Supervision. **Shitan Wang:** Resources. **Yuan Zhao:** Data curation. **Yuquan Liu:** Investigation. **Yongli Gao:** Project administration, Funding acquisition, Writing - review & editing.

Declaration of Competing Interest

The authors declare that they have no known competing financial interests or personal relationships that could have appeared to influence the work reported in this paper.

Acknowledgments

We thank the financial support by the National Key Research and Development Program of China (Grant Nos. 2017YFA0206602) and the National Natural Science Foundation of China (Grant Nos. 11334014 and 51802355). H.X. acknowledges the support by the Natural Science Foundation of Hunan Province (Grant No. 2018JJ3625). Y.G. acknowledges the support by the National Science Foundation (Grant Nos. DMR-1903962, DMR-1303742 and CBET-1437656).

Appendix A. Supplementary data

Supplementary data to this article can be found online at https://doi.org/10.1016/j.rinp.2020.103222.

References

[1] Cao Y, Fatemi V, Fang S, Watanabe K, Taniguchi T, Kaxiras E, et al. Unconventional Superconductivity in Magic-Angle Graphene Superlattices. Nature 2018;556:43–50.
[2] Fuhrer MS, Medhekar NV. Dirac-point photocurrents due to the photothermoelectric effect in non-uniform graphene devices. Nat Nanotechnol 2020;15:241–3.
[3] Wu JB, Lin ML, Cong X, Liu HN, Tan PH. Raman spectroscopy of graphene-based materials and its applications in related devices. Chem Soc Rev 2018;47:1822–73.
[4] Geng PB, Zheng S, Tang H, Zhu RM, Zhang L, Cao S, et al. Transition metal sulfides based on graphene for electrochemical energy storage. Adv Energy Mater 2018;8:1703259.
[5] Po HC, Zou LJ, Vishwanath A, Senthil T. Origin of mott insulating behavior and superconductivity in twisted bilayer graphene. Phys Rev X 2018;8:031089.
[6] Cao Y, et al. Correlated insulator behaviour at half-filling in magic-angle graphene superlattices. Nature 2018;556:80–4.
[7] Schwierz F. Graphene transistors. Nat Nanotechnol 2010;5:487–96.
[8] Li L, Yu Y, Ye GJ, Ge Q, Ou X, Wu H, et al. Black phosphorus field-effect transistors.

Nat Nanotechnol 2014;9:372–7.
[9] Alalq I, Gao J, Wang B, Physical and chemical properties of phosphorus. In Fundamentals and applications of phosphorus nanomaterials, American Chemical Society; 2019; Vol. 1333, p 61–77.
[10] Cho SY, Lee Y, Koh HJ, Jung H, Kim JS, Yoo HW, et al. Superior chemical sensing performance of black phosphorus: comparison with Mos2 and graphene. Adv Mater 2016;28:7020–8.
[11] Tiouitchi G, et al. An easy route to synthesize high-quality black phosphorus from amorphous red phosphorus. Mater Lett 2019;236:56–9.
[12] Xu Y, Shi Z, Shi X, Zhang K, Zhang H. Recent progress in black phosphorus and black-phosphorus-analogue materials: properties, synthesis and applications. Nanoscale 2019;11:14491–527.
[13] Shi Z, Ren XH, Qiao H, Cao R, Zhang Y, Qi X, et al. Recent insights into the robustness of two-dimensional black phosphorous in optoelectronic applications. J Photochem Photobiol, C 2020;43:100354.
[14] Luo X, Feng X, Liu Y, Guo J. Rashba spin-orbit coupling enhanced two-photon absorption and its polarization dependence in monolayer black phosphorus. Opt Express 2020;28:9089–98.
[15] Du YL, Ouyang CY, Shi SQ, Lei MS. Ab initio studies on atomic and electronic structures of black phosphorus. J Appl Phys 2010;107:093718.
[16] Rodin AS, Carvalho A, Castro Neto AH. Strain-induced gap modification in black phosphorus. Phys Rev Lett 2014;112:176801.
[17] Narita S, Akahama Y, Tsukiyama Y, Muro K, Mori S, Endo S, et al. Electrical and optical properties of black phosphorus single crystals. Physica B + C 1983;117:422–4.
[18] Liu H, Du Y, Deng Y, Ye PD. Semiconducting black phosphorus: synthesis, transport properties and electronic applications. Chem Soc Rev 2015;44:2732–43.
[19] Guo S, Zhang Y, Ge Y, Zhang S, Zeng H, Zhang H. 2d V-V binary materials: status and challenges. Adv Mater 2019;31:1902352.
[20] Pei J, Yang J, Yildirim T, Zhang H, Lu Y. Many-Body Complexes in 2d semiconductors. Adv Mater 2019;31:1706945.
[21] Zhang M, Wu Q, Zhang F, Chen LL, Jin XX, Hu YW, et al. 2d Black phosphorus saturable absorbers for ultrafast photonics. Adv Opt Mater 2019;7:1800224.
[22] He D, Wang Y, Huang Y, Shi Y, Wang X, Duan X. High-performance black phosphorus field-effect transistors with long-term air stability. Nano Lett 2019;19:331–7.
[23] Huang Y, Liu XY, Liu Y, Shao Y, Zhang SQ, Fang CZ, et al. Nanostructured multiple-layer black phosphorus photodetector based on localized surface plasmon resonance. Opt Mater Express 2019;9:739–50.
[24] Pang JB, Bachmatiuk A, Yin Y, Trzebicka B, Zhao L, Fu L, et al. Applications of phosphorene and black phosphorus in energy conversion and storage devices. Adv Energy Mater 2018;8:1702093.
[25] Chen X, et al. Widely tunable black phosphorus mid-infrared photodetector. Nat Commun 2017;8:1672.
[26] Xu YJ, Liu CL, Guo C, Yu QH, Guo WL, Lu W, et al. High Performance near infrared photodetector based on in-plane black phosphorus P-N homojunction. Nano Energy 2020;70:104518.
[27] Batmunkh M, Bat-Erdene M, Shapter JG. Black Phosphorus: Synthesis And Application For Solar Cells. Adv Energy Mater 2018;8:1701832.
[28] Bai LY, Sun LQ, Wang Y, Liu ZZ, Gao Q, Xiang HJ, et al. Solution-processed black phosphorus/pcbm hybrid heterojunctions for solar cells. J Mater Chem A 2017;5:8280–6.
[29] Wood JD, Wells SA, Jariwala D, Chen KS, Cho E, Sangwan VK, et al. Effective passivation of exfoliated black phosphorus transistors against ambient degradation. Nano Lett 2014;14:6964–70.
[30] Liu H, Neal AT, Si MW, Du YC, Ye PD. The effect of dielectric capping on few-layer phosphorene transistors: tuning the schottky barrier heights. IEEE Electr Device L 2014;35:795–7.
[31] Perello DJ, Chae SH, Song S, Lee YH. High-performance N-type black phosphorus transistors with type control via thickness and contact-metal engineering. Nat Commun 2015;6:7809.
[32] Liu YD, Cai YQ, Zhang G, Zhang YW, Ang KW. Al-doped black phosphorus P-N homojunction diode for high performance photovoltaic. Adv Funct Mater 2017;27:1604638.
[33] Xie HP, Huang H, Cao NT, Zhou CH, Niu DM, Gao YL. Effects of annealing on structure and composition of Lsmo thin films. Phys B-Condens Matter 2015;477:14–9.
[34] Xie HP, Niu DM, Lyu L, Zhang H, Zhang YH, Liu P, et al. Evolution of the electronic structure of C60/La0. 67sr0. 33mno3 interface. Appl Phys Lett 2016;108:011603.
[35] Liu BX, Xie HP, Niu DM, Wang ST, Zhao Y, Liu YQ, et al. Effect of interfacial interaction on spin polarization at organic-cobalt interface. Org Electron 2020;78:105567.
[36] Liu BX, Xie HP, Niu DM, Huang H, Wang C, Wang ST, et al. Interface electronic structure between au and black phosphorus. J Phys Chem C 2018;122:18405–11.
[37] King DE, Swartz WE. Variable-angle x-ray photoelectron spectroscopic determination of the thickness of the oxide layer on aluminum metal: an advanced undergraduate laboratory experiment. J Chem Educ 1987;64:981.
[38] Salaneck WR, Seki K, Kahn A, Pireaux J-J. Conjugated polymer and molecular interfaces: science and technology for photonic and optoelectronic application. New York: CRC Press; 2001.
[39] Gao YL. Surface analytical studies of interfaces in organic semiconductor devices. Mat Sci Eng R 2010;68:39–87.
[40] Seah MP, Dench W. Quantitative electron spectroscopy of surfaces: a standard data base for electron inelastic mean free paths in solids. Surf Interface Anal 1979;1:2–11.
[41] Xie HP, Liu XL, Lyu L, Niu DM, Wang Q, Huang JS, et al. Effects of precursor ratios and annealing on electronic structure and surface composition of Ch3nh3pbi3 perovskite films. J Phys Chem C 2015;120:215–20.
[42] Kazansky IP, Selyaninov IA, Kuznetsov YI. angle resolved xps of monomolecular layer of 5-chlorobenzotriazole on oxidized metallic surface. Appl Surf Sci 2012;259:385–92.